Opposing shear senses in a subdetachment mylonite zone: Implications for core complex mechanics

Frances J. Cooper,[1,5] John P. Platt,[1] Ellen S. Platzman,[1] Marty J. Grove,[2,3] and Gareth Seward[4]

Received 24 November 2009; revised 23 February 2010; accepted 2 March 2010; published 4 August 2010.

[1] Global studies of metamorphic core complexes and low-angle detachment faults have highlighted a fundamental problem: Since detachments excise crustal section, the relationship between the mylonitic rocks in their footwalls and the brittle deformation in their hanging walls is commonly unclear. Mylonites could either reflect ductile deformation related to exhumation along the detachment fault, or they could be a more general feature of the extending middle crust that has been "captured" by the detachment. In the first case we would expect the kinematics of the mylonite zone to mirror the sense of movement on the detachment; in the second case both the direction and sense of shear in the mylonites could be different. The northern Snake Range décollement (NSRD) is a classic Basin and Range detachment fault with a well-documented top-east of displacement. We present structural, paleomagnetic, geochronological, and geothermometric evidence to suggest that the mylonite zone below the NSRD locally experienced phases of both east- and west-directed shear, inconsistent with movement along a single detachment fault. We therefore propose that the footwall mylonites represent a predetachment discontinuity in the middle crust that separated localized deformation above from distributed crustal flow below (localized-distributed transition (LDT)). The mylonites were subsequently captured by a moderately dipping brittle detachment that soled down to the middle crust and exhumed them around a rolling hinge into a subhorizontal orientation at the surface, producing the present-day NSRD. In this interpretation the brittle hanging wall represents a series of rotated upper crustal normal faults, whereas the mylonitic footwall represents one or more exhumed middle crustal discontinuities (LDTs). **Citation:** Cooper, F. J., J. P. Platt, E. S. Platzman, M. J. Grove, and G. Seward (2010), Opposing shear senses in a subdetachment mylonite zone: Implications for core complex mechanics, *Tectonics*, *29*, TC4019, doi:10.1029/2009TC002632.

1. Introduction

[2] Cordilleran metamorphic core complexes (Figure 1) are typically characterized by a low-angle domiform detachment surface that separates unmetamorphosed rocks cut by brittle normal faults in the hanging wall from metamorphic rocks with ductile fabrics in the footwall. The zone of ductile strain in the footwall may be several hundreds of meters to a few kilometers thick, with strain increasing in intensity upward to a zone of mylonite directly beneath the detachment. The top of the mylonite is overprinted by a narrow zone of cataclastic rocks, above which lies the discrete brittle slip surface of the detachment [*Coney*, 1980; *Davis and Lister*, 1988; *Miller et al.*, 1983].

[3] In some core complexes, the mylonites may represent the ductile downward extension of the detachment, and the upward transition from ductile to brittle deformational structures simply reflects progressive cooling of the footwall during extensional exhumation [e.g., *Armstrong*, 1972, 1982; *Davis and Coney*, 1979; *Davis*, 1983; *Mancktelow*, 1985; *Cottle et al.*, 2007]. On the other hand, *Davis* [1988] and *Lister and Davis* [1989] suggested that the mylonites in the Whipple Mountains core complex of California (Figure 1) represent a zone of mid- to lower crustal deformation that was "captured" and exhumed by a younger detachment that cut down to meet it. In the Whipples, the mylonite zone and the brittle detachment fault separate in the up-dip direction (Figure 2), indicating that they are not directly related, but similar kinematics in the mylonites and on the detachment suggest that both were caused by regional extension in the early Miocene. This concept may be applicable to other core complex mylonites. For example, *Platt and Behrmann* [1986] noted the presence of two mylonitic fabrics beneath a detachment fault in the Betic Cordillera, Spain: a zone of relatively high temperature mylonite at depth below the detachment, truncated by a lower temperature ultramylonite adjacent to the detachment. Similarly, a recent study by *Johnston et al.* [2007] of the Nordfjord–Sogn Detachment Zone in Norway suggests that mylonitic deformation predated initiation of the detachment, and the mylonites were subsequently truncated and partially exhumed by it.

[1]Department of Earth Sciences, University of Southern California, Los Angeles, California, USA.
[2]Department of Earth and Space Sciences, University of California, Los Angeles, California, USA.
[3]Now at School of Earth Sciences, Stanford University, Stanford, California, USA.
[4]Department of Earth Science, University of California, Santa Barbara, California, USA.
[5]Now at School of Earth and Space Exploration, Arizona State University, Tempe, Arizona, USA.

0278-7407/10/2009TC002632

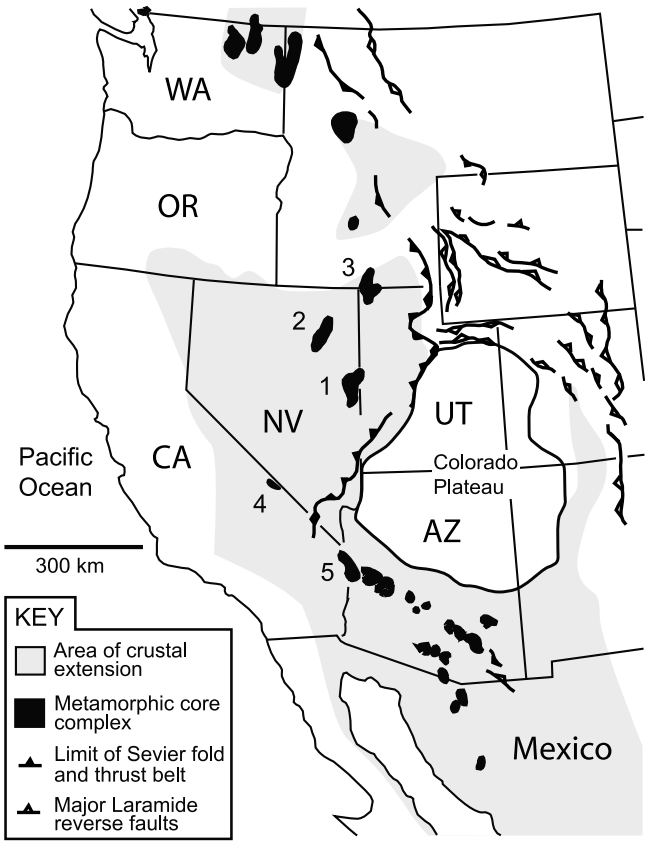

Figure 1. The North American Cordillera. Metamorphic core complexes form a semicontinuous north–south belt from Canada to Mexico in the hinterland of the Sevier thrust belt: 1, Snake Range; 2, Ruby Mountains–East Humboldt Range; 3, Raft River Mountains; 4, Funeral Mountains; 5, Whipple Mountains. Redrawn from the study by *Wong* [2008], modified from the studies by *Coney* [1980] and *Wernicke* [1992].

[4] The preservation of this older and deeper zone of mylonitic deformation beneath detachments provides an opportunity to examine how the mid- to lower crust responds to extensional strain. In particular, is deformation distributed or localized, coaxial or uniaxial? In the Basin and Range Province, *Wernicke* [1981] originally proposed that extension is dominated by simple shear along low-angle normal faults that penetrate the whole crust. However, the presence of a flat Moho, the limited spacing of normal faults, and the restriction of seismicity to the upper crust have led to the consensus that the middle-lower crust in this area behaves as a viscous fluid, with extension dominated by distributed, coaxial deformation [e.g., *Eaton*, 1982; *McKenzie et al.*, 2000].

[5] Here we document the kinematic history of a section of the well-exposed mylonite zone in the northern Snake Range in eastern Nevada (Figure 1). Our aim is to establish how this mylonite zone formed and evolved during crustal extension and exhumation and consider the implications that this history has for the evolution of the Snake Range metamorphic core complex and for mechanisms of crustal extension as a whole.

2. The Northern Snake Range Mylonite Zone

[6] The northern Snake Range is a classic example of a Cordilleran metamorphic core complex, comprising a domiform detachment surface (the northern Snake Range décollement, NSRD) that divides the range into a non-metamorphic upper plate of Paleozoic shale, limestone, and dolomite, which have been greatly extended by slip on brittle normal faults, and a lower plate of metamorphosed Upper Precambrian to Lower Cambrian schist, quartzite, and marble intruded by Jurassic and Cretaceous granitic plutons and Tertiary dikes, which have been affected by substantial ductile strain [*Coney*, 1974, 1980; *Hose et al.*, 1976; *Miller et al.*, 1983; *Misch and Hazzard*, 1962; *Misch*, 1960] (Figures 3 and 4).

[7] Northern Snake Range footwall rocks record two phases of deformation and metamorphism. First, a late Cretaceous contractional event related to Sevier thrust faulting [*Miller and Gans*, 1989] buried them to a depth of around 30 km [*Lewis et al.*, 1999] and produced a penetrative foliation and greenschist to amphibolite-grade metamorphism; second, a Tertiary extensional event related to footwall exhumation produced a subhorizontal mylonitic foliation and corresponding retrogressive metamorphic overprint [*Gans and Miller*, 1983; *Lee et al.*, 1987]. The northern Snake Range mylonite zone is a >100 m thick high-strain zone beneath the NSRD, defined by a subhorizontal mylonitic foliation and a consistent ESE-trending stretching lineation (Figure 5) [*Gaudemer and Tapponnier*, 1987; *Lee et al.*, 1987; *Miller et al.*, 1983]. The mylonite zone is generally interpreted to be a Tertiary feature related to extension and exhumation along the NSRD, but it decreases in intensity from east to west, disappearing completely in the northwestern part of the range [*Lee et al.*, 1987; *Miller et al.*, 1983]. $^{40}Ar/^{39}Ar$ cooling ages [*Lee and Sutter*, 1991; *Lee*, 1995] denote a systematic increase in the age of exhumation from 20 Ma in the east to 50 Ma in the west, suggesting that ductile deformation in the western part of the range is likely to be Eocene or older (Figure 3).

[8] To better constrain the evolution of the mylonite zone, we conducted a detailed kinematic and structural study in Marble Wash in the northeastern corner of the range (Figure 3). The aim of this study is to use kinematic criteria to distinguish between deformation that could be related to slip on the detachment and deformation that could have resulted from midcrustal extensional deformation before

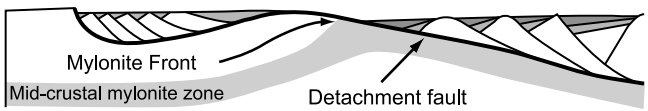

Figure 2. "Capture" of a midcrustal mylonite zone by a down-cutting normal fault. The mylonite front marks the separation between the detachment fault and the underlying mylonite zone. From the study by *Axen and Bartley* [1997], after *Lister and Davis* [1989].

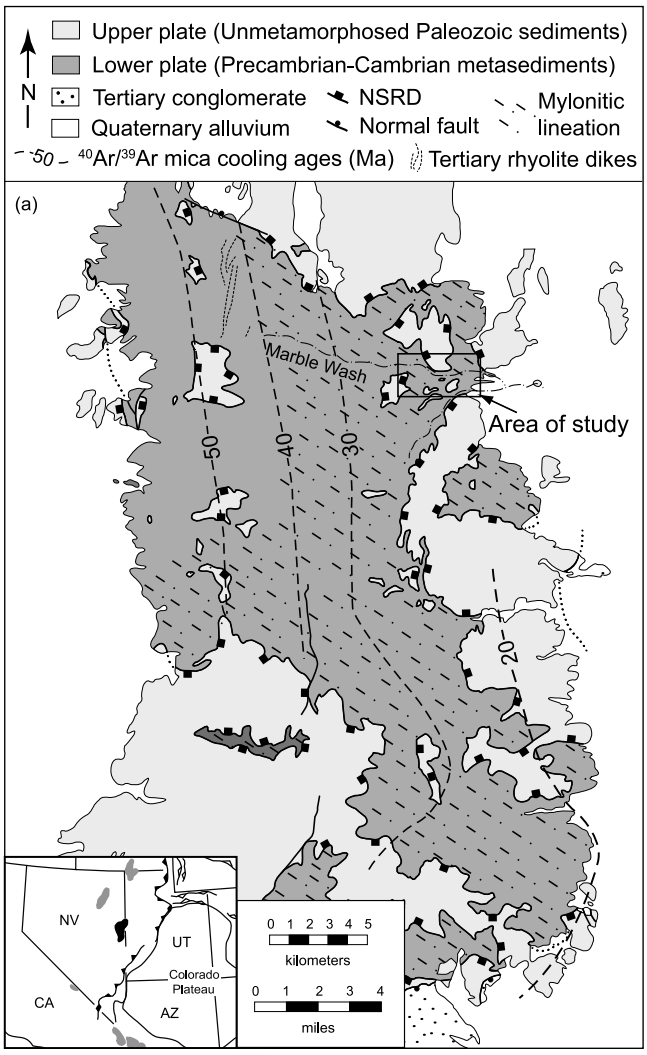

Figure 3. Simplified geologic map of the northern Snake Range metamorphic core complex showing the area of study, Marble Wash. Dashes represent the WNW-ESE mylonitic stretching lineation. N-S trending contours indicate K-Ar and $^{40}Ar/^{39}Ar$ mica cooling ages from the studies by *Lee and Sutter* [1991], *Lee* [1995], and *Miller et al.* [1988]. The Tertiary rhyolite dike swarm is dated at 36.9 ± 0.3 Ma ($^{40}Ar/^{39}Ar$ on muscovite), interpreted as an intrusive age [*Lee and Sutter*, 1991].

formation of the detachment. Marble Wash is an ideal study location for three reasons: (1) its gentle eastward slope follows the structural level of the décollement for ~3 km; (2) it trends east to west, roughly parallel to the WNW-ESE stretching lineation found throughout the footwall; and (3) in this area, the detachment cuts up-section out of the Precambrian to Cambrian quartzites and schists that dominate most of the range and into overlying Middle Cambrian to Ordovician marbles and calcareous mica schists that have been intruded by mafic dikes. The rheological contrasts between the marbles, calcareous mica schists, and mafic dikes have produced heterogeneous deformation within the wash, including ductile faults, folds, and boudins that provide good strain markers and kinematic indicators for structural analyses. In addition, the mafic dikes present a good opportunity to place paleomagnetic and geochronological constraints on the deformation.

[9] Deformation in the mylonitic rocks of the northern Snake Range is controversial because there is evidence for both coaxial and noncoaxial shear. *Lee et al.* [1987] used mesoscopic and microstructural evidence from a transect across the southern part of the range to propose that the lower plate was deformed during an early period of coaxial deformation followed by a later component of noncoaxial top-east shear accompanied by pure shear stretching on the eastern flank of the range. On the other hand, a structural study by *Gaudemer and Tapponnier* [1987] that spanned both northern and southern parts of the range suggested that lower plate deformation occurred entirely by noncoaxial, top-east shear. In Marble Wash, the situation is complicated by evidence for both east- and west-directed phases of shear. These observations have previously been interpreted as either conjugate shear bands formed during coaxial extension [*Lee et al.*, 1999] or localized west-dipping shear bands associated with perturbations in the wake of asymmetric boudins [*Gaudemer and Tapponnier*, 1987]. New observations presented here suggest that these west-directed shear zones are not minor local features but important structures that cut and overprint earlier east-directed shear zones and thus have important implications for the evolution of the northern Snake Range metamorphic core complex.

3. Kinematics

3.1. Structural Observations

[10] Over an east–west distance of 3 km, Marble Wash exposes an intensely deformed section of Cambrian carbonate rocks with layers of calcareous mica schist and dolostone boudins up to several tens of meters long. In one section of the wash, the calcareous rocks are cut by three mafic dikes (Figure 6; 39°7′35″N, 114°7′35″W) that highlight significant structural relationships. We therefore focused our study on this section, although the structures described are found throughout the 3 km long section in the wash.

[11] The Cambrian carbonates in this area reveal little of their history before mylonitization deformation, apart from some areas of large-scale isoclinal folding near the crest of

Figure 4. (a) Simplified geologic map of the northern Snake Range compiled from 1:24,000-scale mapping by *Gans et al.* [1999a, 1999b], *Lee et al.* [1999a, 1999b, 1999c], *Miller and Gans* [1999], and *Miller et al.* [1999]. (b) Simplified geologic cross section across the northern part of the range, including the Marble Wash dikes to the east and the rhyolite dike swarm to the west. The lower plate contains a large-scale recumbent syncline formed by Cretaceous contraction and later modified by Tertiary extensional strain. Modified from studies by *Lee et al.* [1999a, 1999b].

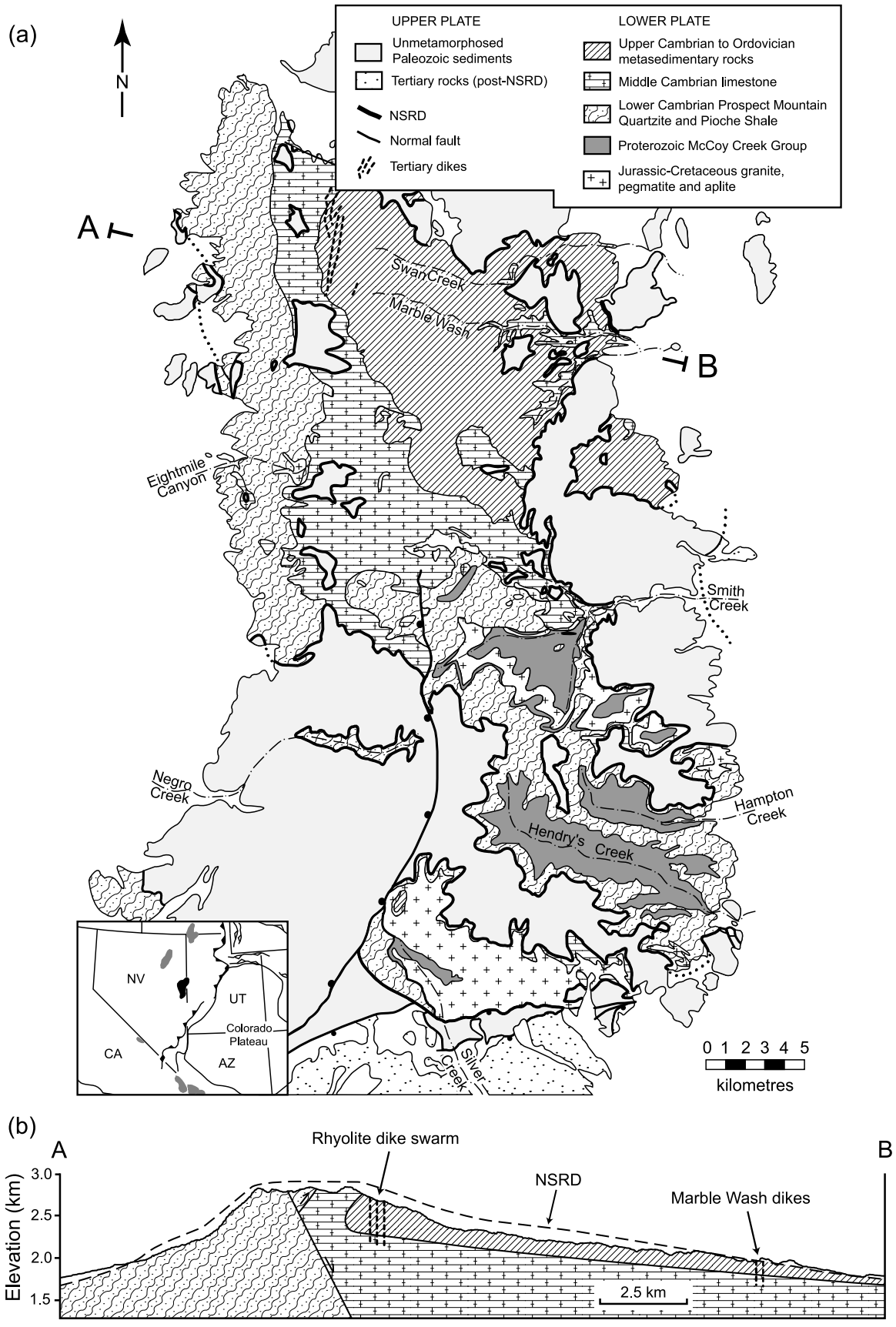
(a)
N
UPPER PLATE
Unmetamorphosed Paleozoic sediments
Tertiary rocks (post-NSRD)
NSRD
Normal fault
Tertiary dikes
LOWER PLATE
Upper Cambrian to Ordovician metasedimentary rocks
Middle Cambrian limestone
Lower Cambrian Prospect Mountain Quartzite and Pioche Shale
Proterozoic McCoy Creek Group
Jurassic-Cretaceous granite, pegmatite and aplite
A
B
Swan Creek
Marble Wash
Eightmile Canyon
Smith Creek
Negro Creek
Hampton Creek
Hendry's Creek
Silver Creek
NV
UT
Colorado Plateau
CA
AZ
0 1 2 3 4 5
kilometres
(b)
A
B
Rhyolite dike swarm
NSRD
Marble Wash dikes
Elevation (km)
3.0
2.5
2.0
1.5
2.5 km

Figure 4

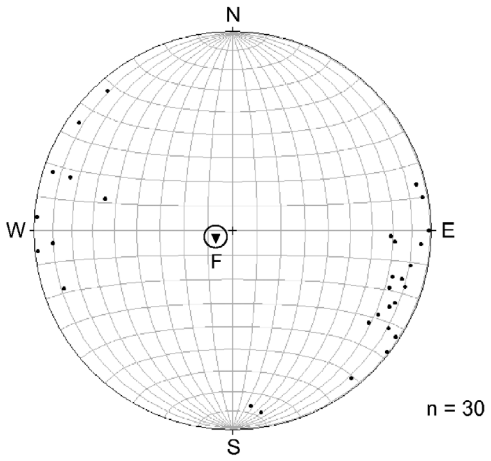

Figure 5. Equal-area projection of 30 stretching lineations measured in Marble Wash. F, pole to the mean mylonitic foliation (30 measurements) with a 95% confidence circle.

the range, which are most likely related to Late Cretaceous Sevier contraction (Figure 4b) [*Lee et al.*, 1999a, 1999b]. In Marble Wash, a subhorizontal mylonitic foliation that is cut by the mafic dikes can locally be distinguished (Figure 5). This foliation is defined by transposed layering, attenuated isoclinal folds, and sheath folds, and carries an ESE-trending stretching lineation. The microstructure, however, is characterized by millimeter-sized equant grains, suggesting relatively high temperature annealing, and we have not been able to determine a sense of shear.

[12] Both the early foliation and the dikes have been overprinted by a phase of intense east-directed shear. This produced east-dipping shear bands (Figures 7a and 7b) on various scales, which intensify into more than 10 m thick detachment-parallel zones of calcareous mylonite containing asymmetric dolomite and mica porphyroclasts (Figures 7c and 7d). The mylonites carry an ESE-trending stretching lineation and contain zones of intense folding. The folds vary in geometry from tight but coherent folds with north–south hinge lines and top-east asymmetry to highly attenu-

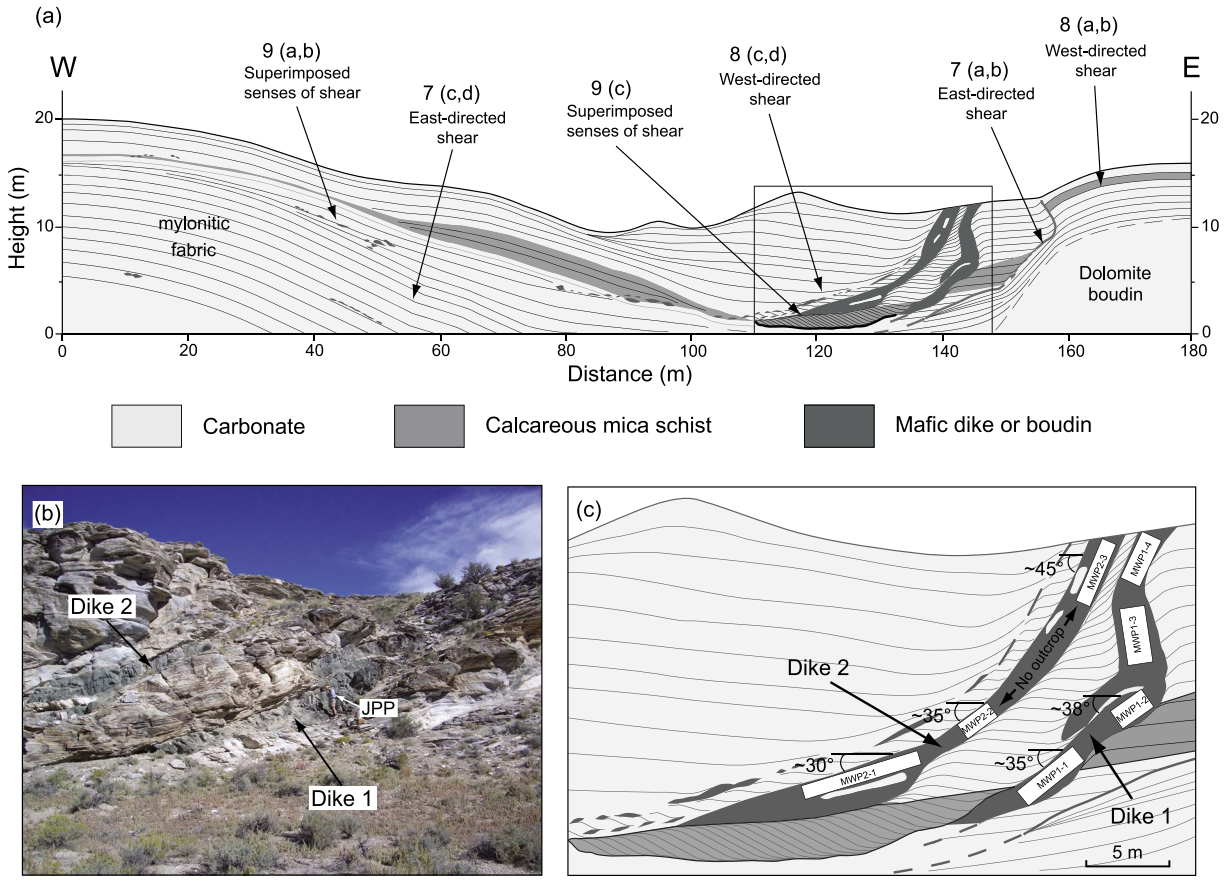

Figure 6. (a) The primary area of study (39°7′35″N, 114°7′35″W): a 180 m long section of the north wall of Marble Wash containing three basaltic dikes (the easternmost dike was too thin for sampling and analysis). Deformation is highlighted by a calcareous schist marker horizon that is deflected across the dikes. Labels (e.g., 9a,b) refer to figure numbers in this paper. (b) Photograph of the two wider mafic dikes cross-cutting the dominant mylonitic foliation. One of the authors (JPP) is included for scale. (c) Enlargement of the dikes from Figure 6a showing paleomagnetic sampling localities. MWP, Marble Wash Paleomagnetic sample.

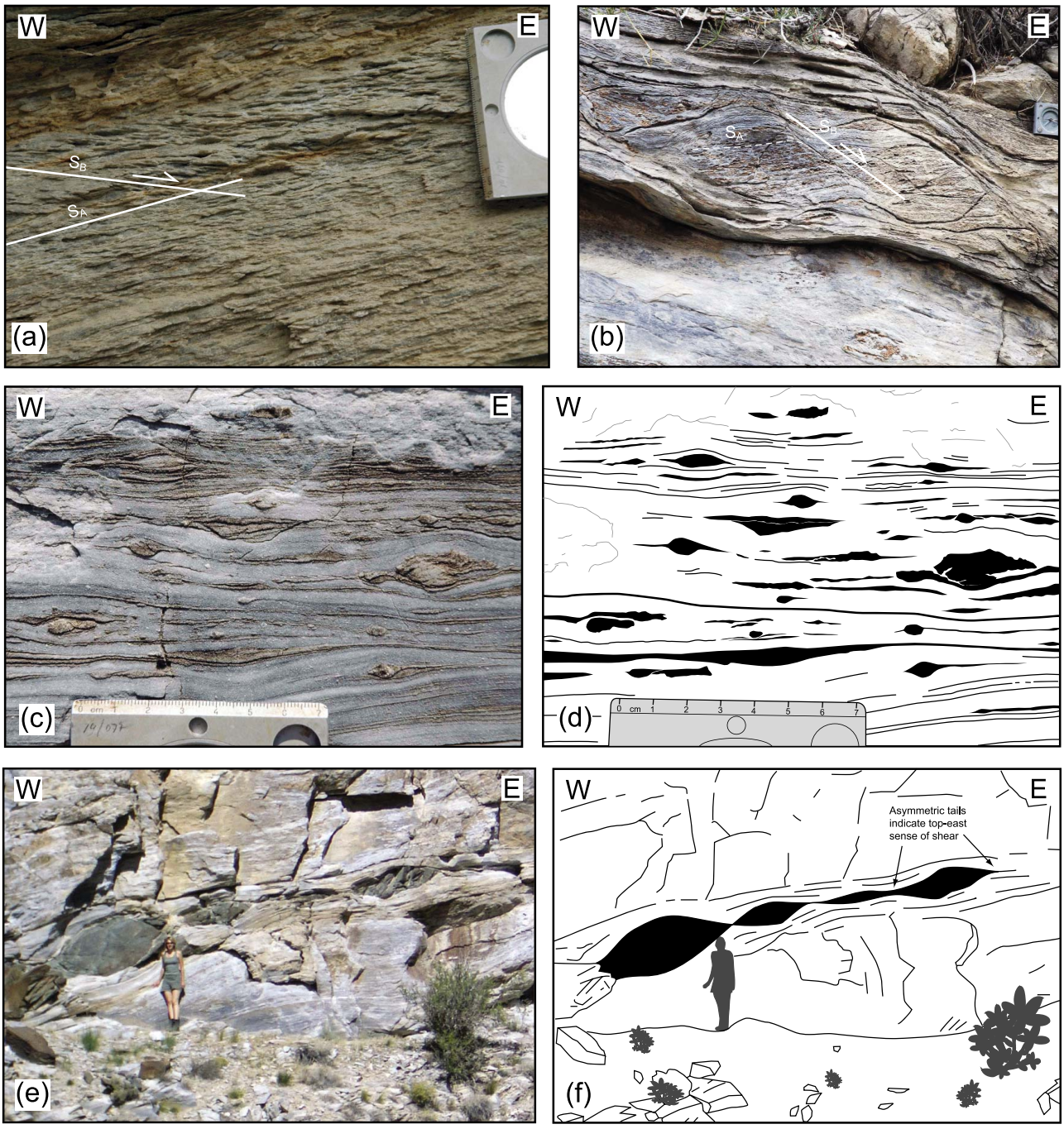

Figure 7. Evidence for east-directed shear in calcareous mylonites. (a) The dominant mylonitic foliation (S_A) is cut by an east-dipping fabric (S_B), formed by a series of closely spaced shear bands that define a cleavage. Sense of shear in the shear bands is indicated in thin section by an oblique grain-shape fabric within the recrystallized grains and by deflection of calcite twins. (b) East-dipping shear bands (S_B) deflect the mylonitic foliation (S_A). (c) Photograph and (d) line drawing of top-east asymmetric dolomite porphyroclasts within a calcite matrix. (e) Photograph and (f) line drawing of a train of asymmetric top-east mafic dike boudins. One of the authors (FJC) is included for scale.

ated folds with sheared out limbs and variably oriented hinge lines, some of which are subparallel to the stretching lineation. Some of the small-scale folds are east-vergent with extreme attenuation of the long limbs and short limbs, which roll over into geometries resembling delta-type porphyroclasts with a top-east sense of shear. Dikes in these high-strain zones are transposed into the mylonitic foliation and pulled apart into boudins that have developed east-

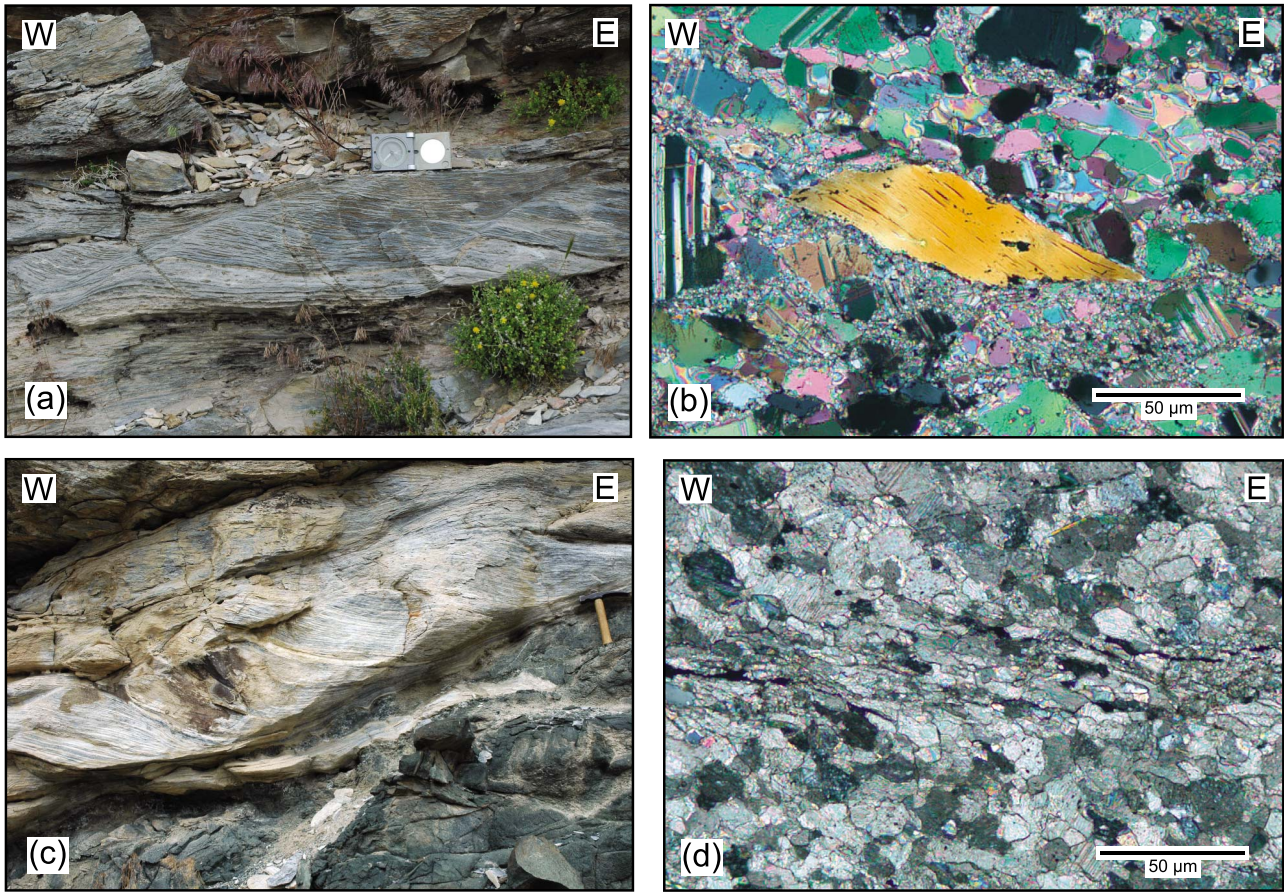

Figure 8. Evidence for west-directed shear in calcareous mylonites. (a) West-directed shear bands deflect the mylonitic fabric into a sigmoidal pattern. (b) Photomicrograph from the same location contains mica fish that show a clear top-west shear sense. (c) West-directed shear bands along the margin of a mafic dike. (d) Photomicrograph of a west-dipping shear band from the same location with a shape fabric in recrystallized calcite creating a sigmoidal fabric pattern.

vergent tails (Figures 7e and 7f). On the microscale, calcite in the east-directed shear band has been dynamically recrystallized to a grain size of 100 μm or less with an oblique grain shape fabric that indicates top-east shear.

[13] All these structures are cut by 1 cm to 10 m wide west-dipping and west-directed shear bands that deform the dikes and form top-west asymmetric porphyroclasts within the main fabric. Figures 8a and 8c show west-directed shear bands that cut the earlier mylonitic foliation. In Figure 8c the shear bands have formed along the margin of one of the mafic dikes, suggesting that, in this instance, the dike localized the deformation. However, west-directed structures can also be found away from the dikes, and a large west-directed shear zone was found 1 km further west along the wash. Figures 8b and 8d illustrate this west-directed deformation at the microscale. Occasional grains of metamorphic muscovite form fish showing a top-west sense of shear (Figure 8b). Within the shear bands, the shape fabric defined by dynamically recrystallized calcite forms a sigmoidal pattern that indicates a top-west shear sense (Figure 8d).

[14] The shear bands shown in Figure 8 transfer displacement westward onto earlier detachment-parallel east-directed shear zones, creating complicated structures that represent the superposition of east- and west-directed shear (e.g., Figure 9). Figure 9a shows a dike that was boudinaged and cut by a top-east fault and then folded over and sheared to the west. The upper limb of this fold has been greatly thinned, suggesting that it has experienced considerable west-directed shear strain. Figure 9b illustrates the complex deformation within this west-directed shear zone, which comprises a small folded boudin and two asymmetric boudins with opposing senses of shear. Figure 9c shows the complicated fabric relationships that formed where west-directed shear was superposed on earlier east-directed structures. Both the mylonitic fabric and the closely spaced east-directed shear bands are cut and offset by a later west-directed shear band.

[15] We were not able to distinguish phases of deformation on the basis of statistically defined orientation of the foliation or lineation. The calcite rocks develop a composite foliation in most places, the orientation of which varies as a result of deflection around rigid dolostone boudins, adjacent to the dikes, and in the east- and west-directed shear zones. The stretching lineation is consistently ESE-trending

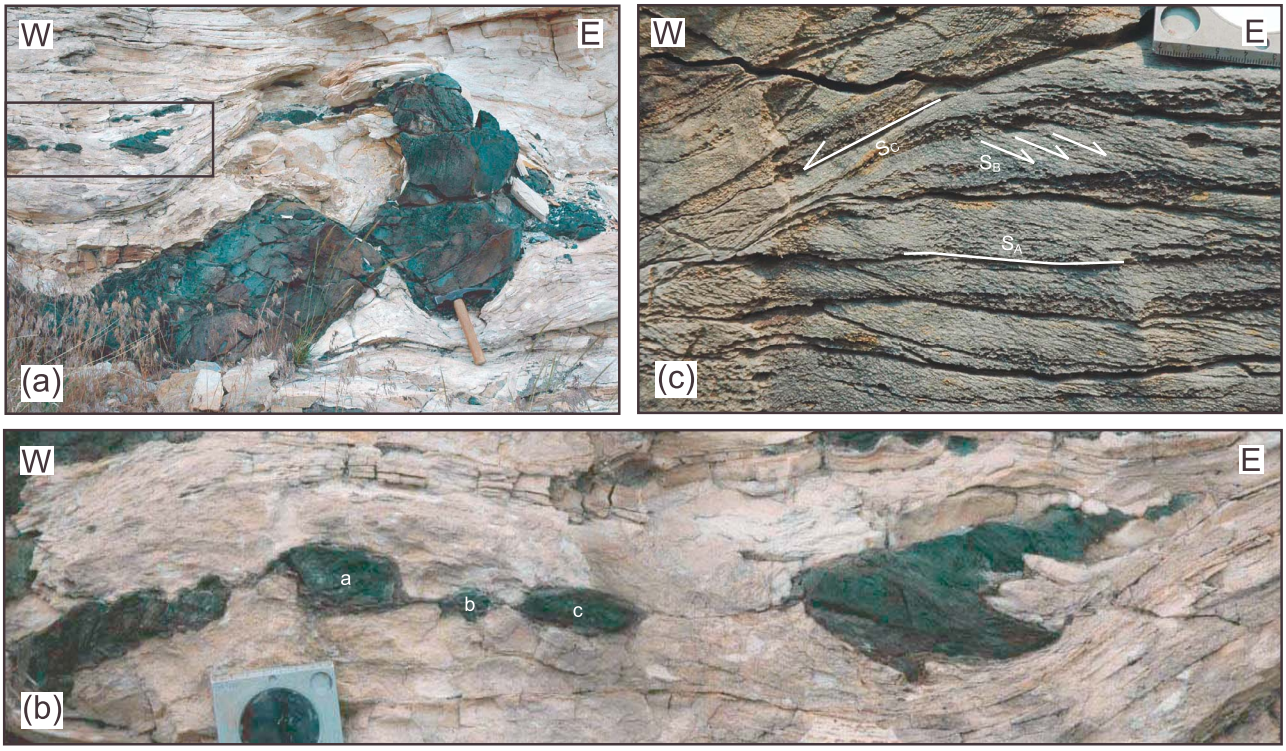

Figure 9. Relationships between east- and west-directed shear structures. (a) Boudinaged dike that has experienced later folding and top-west shear. (b) Detailed view of the sheared boudin showing complicated geometries where west-directed shear structures overprint east-directed structures. Boudins are folded and show opposing senses of shear: Boudin a is top-west, whereas boudins b and c are top-east. (c) Subhorizontal mylonitic foliation (S_A) and east-dipping shear bands (S_B) are both cut and deflected by a later west-dipping shear band (S_C).

(Figure 5). We have distinguished the phases of deformation described here based on their structural relationship to the dikes and on the sense of shear.

3.2. Paleomagnetic Constraints

[16] In addition to the structural observations, the deformed mafic dikes provide an opportunity to place paleomagnetic constraints on both vertical and horizontal axis rotations within the mylonite zone. The mafic dikes in this predominantly east-vergent mylonite zone are highly deformed and west-dipping, which raises questions about their emplacement history and their relationship to the evolution of the zone. Two possibilities are (1) the dikes were intruded vertically and then rotated top-east in an east-vergent shear zone or (2) were intruded into west-dipping extension fractures that opened during the period of west-directed shear within the zone and have not been significantly rotated since. To differentiate between these two possibilities, we carried out a paleomagnetic study of both dikes to determine the orientation and magnitude of postemplacement dike rotation.

3.2.1. Methods

[17] Samples for magnetic analysis were collected from multiple sites on each of the mafic dikes (Figure 6c) using a portable gasoline-powered rock drill. Where possible, samples were drilled close to the chilled margin and in the center of the dikes to check for magnetic homogeneity. Eighteen cores were collected from dike 1 and 15 cores were collected from dike 2 to allow for statistical analysis. The cores were oriented by using a Brunton compass and an orienting platform that includes a Sun compass for magnetically strong samples. Standard cylindrical cores of 2.5 cm diameter and 10 cm length were later cut into 2.25 cm long samples.

[18] The dikes have a primary mineral assemblage of fine- to medium-grained hornblende + biotite + plagioclase ± quartz, overprinted by chlorite during later greenschist metamorphism (Figure 10). Samples collected for paleomagnetic analysis have an undeformed crystalline igneous texture and correspondingly low anisotropies of magnetic susceptibility of ~1.01%–1.02% (Table 1).

[19] Samples were analyzed using a 2G cryogenic magnetometer at Occidental College, Los Angeles, CA. The stable characteristic components of remanent magnetization (ChRM) were isolated using stepwise thermal and alternating field (AF) demagnetization procedures. During the thermal demagnetization procedure, each sample was typically demagnetized with 50°C steps below 500°C and then 25°C steps until the intensity of magnetization fell below the measuring range of the magnetometer. Stepwise AF demagnetization was carried out with 2.5 mT steps from 0 to

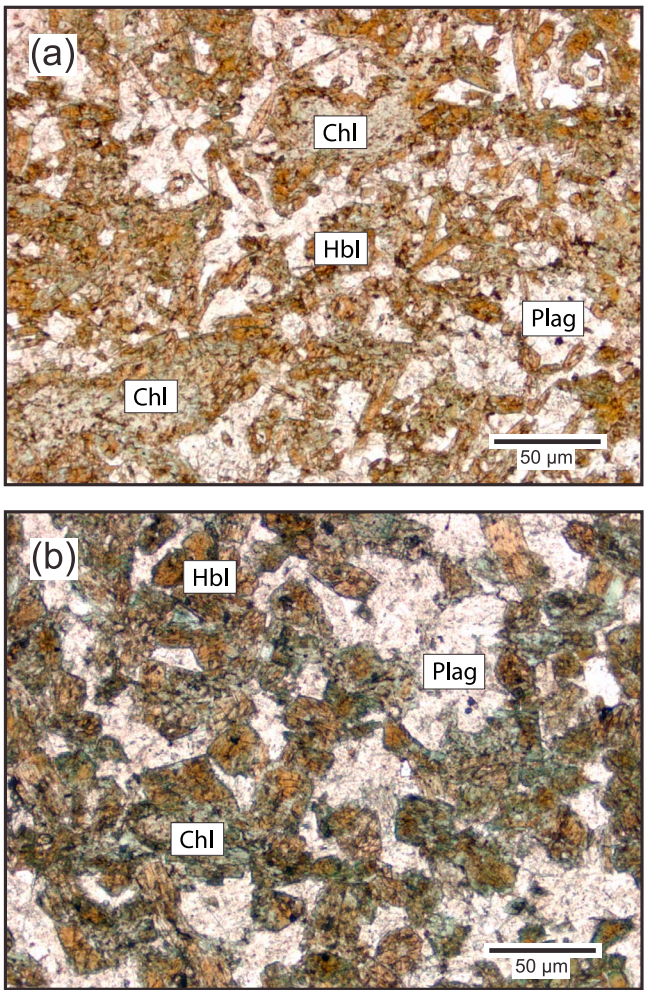

Figure 10. Thin-section photomicrographs of (a) dike 1 and (b) dike 2 (see Figure 6) in plane-polarized light illustrate the crystalline igneous texture of the samples. Chl, chlorite; Hbl, hornblende, and Plag, plagioclase.

5 mT, 5 mT steps from 5 to 40 mT, and 10 mT steps from 40 to 140 mT (Figure 11).

3.2.2. Results

[20] Natural remanent magnetization (NRM) intensities were relatively weak (10^{-5} A/m), consistent with the metamorphic grade and weathering that the dikes have experienced. Both thermal and AF demagnetization procedures produced a relatively simple NRM consisting of two overlapping components of remanent magnetization. The lowest temperature component was usually isolated below 200°C, with a direction subparallel to the present geomagnetic field at the sample site. We therefore interpret this as a recent viscous overprint. AF demagnetization produced a similar result, with the lowest coercivity component demagnetizing below 25 mT.

[21] In the majority of samples, the ChRM was isolated between the maximum blocking temperature of the low-temperature component and 575°C (Figure 11a). AF demagnetization produced a similar result, with the high-coercivity component demagnetizing between 30 and 140 mT (Figure 11b). In both cases, samples were not completely demagnetized, suggesting that the samples have a higher temperature, higher coercivity component. This result, combined with rock magnetization experiments carried out at the paleomagnetic laboratory at the University of Southern California, Los Angeles (USC), suggests that the ChRM is carried primarily by small, single-domain grains of magnetite, but a high-temperature, high-coercivity component is also active, most likely a result of the presence of hematite.

[22] The mean ChRM for each sampling site on the dikes is given in Table 1. This shows that the ChRM for dike 1 has an average declination of 331.2° and inclination of 54.9°, whereas dike 2 has a slightly shallower ChRM of 319.4° and 45.1°, respectively.

3.2.3. Dike Geochronology

[23] Mafic rocks are notoriously difficult to date because silica undersaturation of the melt leads to little or no zircon crystallization. If zircons are present, they are usually inherited or simply too small to extract by typical mineral separation procedures. However, with the advent of high-resolution techniques such as secondary ionization mass spectrometry by ion probe, it is now possible to carry out in situ analyses of small (≤30 μm) zircon crystals.

[24] Ten polished thin sections (five from each dike) were made from offcuts of the paleomagnetic dike cores. A map of each thin section was made using a LEO 1430VP scanning electron microscope. The majority of zircons identified were ≤10–15 μm in diameter, smaller than the diameter of the ion beam, but about 150 grains were large enough (≥15–

Table 1. Remanent Magnetization Parameters

Site	N	ChRM (Dec/Inc)	n	α_{95}	k	AMS % Anisotropy	Dike Strike/Dip
MWP1-1	8	326.4°/54.4°	6	7.39	50.1	1.03	016°/40°W
MWP1-2	5	332.2°/52.4°	4	7.90	101.76	1.03	016°/42°W
MWP1-3	6	339.9°/63.8°	5	6.80	101.98	1.04	347°/76°E
MWP1-4	7	326.3°/49.0°	6	6.10	100.64	1.04	358°/30°W
MWP2-1	6	311.0°/40.9°	5	4.39	243.48	1.01	016°/30°W
MWP2-2	7	318.1°/42.7°	6	3.20	355.66	1.01	020°/35°W
MWP2-3	8	329.0°/51.7°	7	3.8	216.16	1.02	015°/44°W

N, number of samples demagnetized; ChRM (Dec/Inc), declination and inclination of the high-temperature component of remanent magnetization in geographic coordinates; *n*, number of samples used to calculate site mean; α_{95}, Fischer 95% confidence angle; *k*, Fischer precision parameter; AMS % anisotropy, percent anisotropy of magnetic susceptibility. MWP, Marble Wash Paleomagnetic sample.

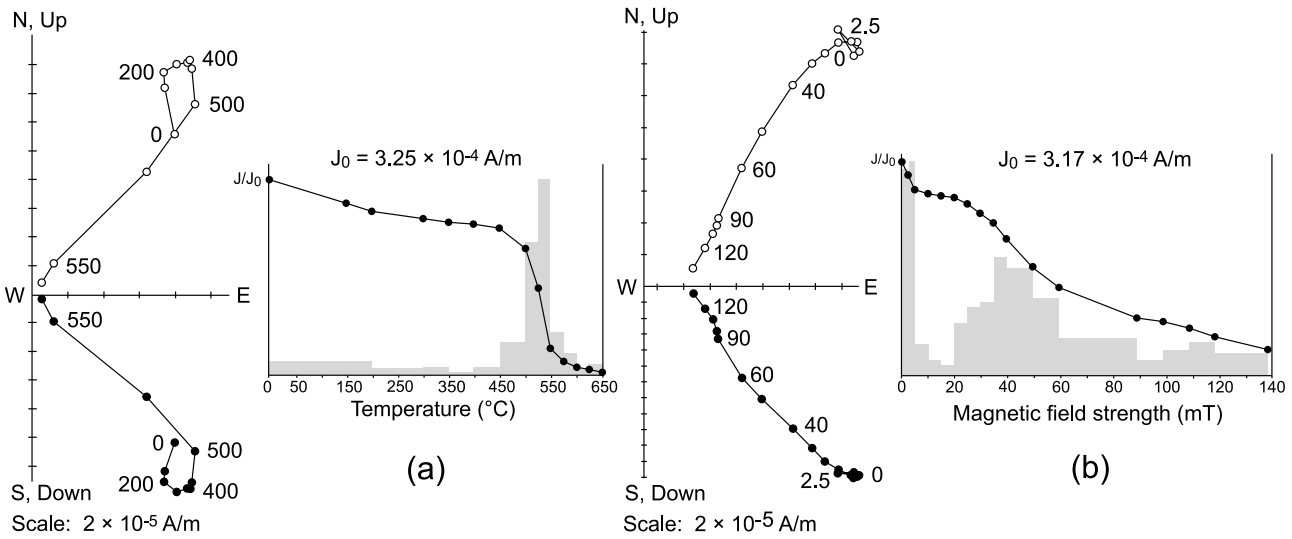

Figure 11. Typical vector diagrams and intensity decay curves for site MWP2-1 samples undergoing (a) thermal (°C) and (b) alternating field (mT) demagnetization. Vector diagrams are in geographic coordinates. Open circles indicate projection of the natural remanent magnetization (NRM) onto the horizontal plane, solid dots indicate projection of the NRM onto the vertical plane. J, NRM intensity; J_0, initial NRM intensity. MWP, Marble Wash Paleomagnetic sample.

30 μm) to be analyzed. Of these, 21 were selected for analyses (5 from dike 1 and 16 from dike 2). These zircons are irregular in shape (Figure 12a) but euhedral, suggesting magmatic rather than metamorphic growth. In addition, they contain high U and Th concentrations (7,800 and 25,700 ppm, respectively), which also points to a magmatic origin because Th is highly mobile in the presence of fluid.

[25] Before the ion microprobe analysis, grain mounts were cleaned in 1 N HCl solution to reduce common Pb contamination and coated with ~100 Å of Au to facilitate conductivity. We performed 25 U/Pb analyses using a Cameca IMS1270 high-resolution ion microprobe at the W.M. Keck Foundation Center for Isotope Geochemistry at the University of California-Los Angeles (UCLA). Ion intensities were measured in 10–15 cycles using a mass-filtered O^- primary ion beam of 4.5 nA focused to a $\leq$10 μm spot. AS-3 [*Black et al.*, 2003; *Paces and Miller*, 1993] reference zircons were used to calibrate U, Th, and Pb sensitivities. The zircons analyzed gave a middle Eocene $^{238}U/^{206}Pb$ age of 40.4 ± 1.4 Ma (2σ; mean square weighted deviation = 4.5). All ages were calculated using the Isoplot software package [*Ludwig*, 2001] and are reported at the 2σ confidence level (Figure 12b).

3.2.4. Reconstructing the Dikes

[26] To reconstruct the initial orientation of the dikes, both the declination and inclination of the mean remanence observed in each sampling site were compared with the expected field direction for the middle Eocene (declination = 346.1°, inclination = 58.69°) calculated from the combined observational and synthetic polar wander curves of *Besse and Courtillot* [1991]. Figure 13 illustrates the method used to reconstruct dike 2. In Figure 13a, ChRM directions, the middle Eocene expected direction, and the orientations of the dike margins for each of the three dike 2 sampling sites are plotted on an equal-area projection. For reference, the mean foliation and WNW-ESE stretching lineation are also plotted. The three ChRM directions line up along a small circle with a horizontal north–south axis, together with the expected direction; the poles to the dike margins line up along a separate small circle, but also with a horizontal north–south axis. The original orientation of the dikes was determined by rotating each ChRM direction and corresponding dike margin by the same amount about the north–south axis until the ChRM directions overlapped the middle Eocene expected direction (Figure 13b). At this point, the dike margin orientations coincided to give a single original dike margin orientation of 011°W/60°W (Figure 13b). Figure 13c provides a schematic illustration of this rotation.

[27] On the basis of this reconstruction, we conclude that dike 2 has experienced little or no vertical axis rotation, and 15°–30° of top-east rotation, although the total amount of top-east rotation may have initially been greater and subsequently undone by top-west rotation. This result implies that the dike was not intruded into a west-dipping extension fracture during a period of west-directed shear; therefore, the west-directed phase of deformation must postdate emplacement of the dikes at 40.4 Ma.

[28] A similar attempt at reconstructing dike 1 proved unsuccessful because of unstable paleomagnetic results. This most likely reflects the higher degree of alteration and chloritization exhibited by dike 1, which could be a function of its smaller grain size.

4. Temperature and Timing of Deformation

[29] Constraining the temperature and timing of the different phases of mylonitic deformation is crucial to understanding how the mylonite zone formed. Here we combine new calcite-dolomite thermometry and electron backscatter

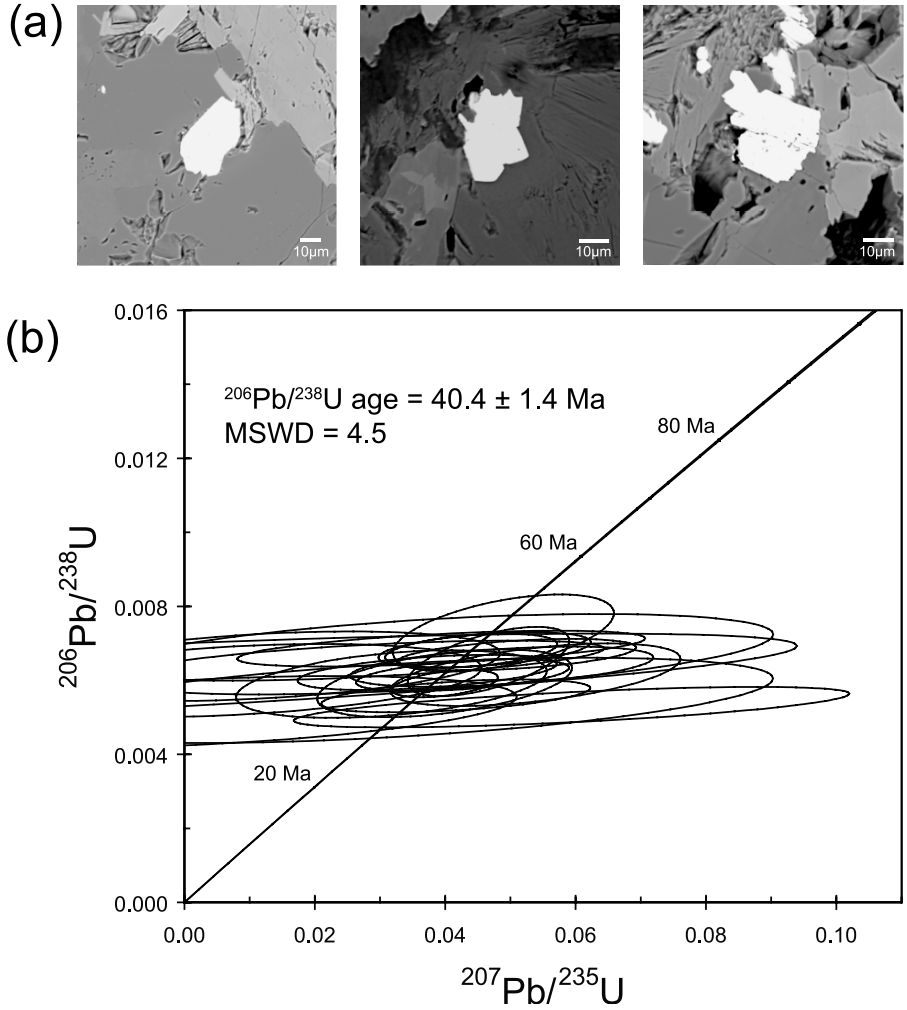

Figure 12. (a) Backscattered electron images of selected zircons. (b) Concordia plot with in situ U/Pb ion probe results. Regression of U/Pb data indicates a ^{238}U/^{206}Pb age of 40.4 ± 1.4 Ma (2σ; mean square weighted deviation [MSWD] = 4.5).

diffraction data with published ^{40}Ar/^{39}Ar and fission track thermochronology to build a coherent picture of mylonite zone evolution.

4.1. Temperature

4.1.1. Calcite-Dolomite Thermometry

[30] The coexistence of quartz and dolomite in the Cambrian carbonate rocks of Marble Wash suggests that mylonitic deformation occurred at temperatures <500°C [*Winter*, 2001] and that these rocks did not reach amphibolite facies conditions during Cretaceous peak metamorphism, in contrast to the more deeply exhumed Proterozoic rocks in the southern part of the range [*Lewis et al.*, 1999].

[31] To place tighter constraints on the temperature of mylonitic deformation, and in particular on the different phases of deformation, we carried out calcite-dolomite thermometry on samples containing both east- and west-directed structures. Analytical work was carried out on the JEOL JXA-8200 electron microprobe at UCLA. Adjacent calcite and dolomite grains were located from 1 μm resolution X-ray composition maps of Ca and Mg created with an accelerating voltage of 15 kV and a beam current of 100 nA. Grains were then analyzed with an accelerating voltage of 15 kV and a beam diameter of 10 μm to avoid crystal damage. Oxide weight percentages were calculated with JEOL software, which uses ZAF corrections (Z, atomic number; A, absorption; and F, fluorescence) for matrix effects, except for CO_2, which was determined from stoichiometry. Temperatures were calculated using the calcite-dolomite geothermometer of *Anovitz and Essene* [1987].

[32] The results shown in Table 2 indicate that there is a difference in temperature of about 80°C between the two phases of deformation, with top-east shear occurring at 433°C ± 33°C and top-west shear at 351°C ± 20°C. This is consistent with our interpretation that the west-directed deformation happened later and indicates that both phases occurred under conditions in which calcite is ductile.

4.1.2. Electron Backscatter Diffraction

[33] Electron backscatter diffraction (EBSD) analyses were carried out on the same two samples used for the

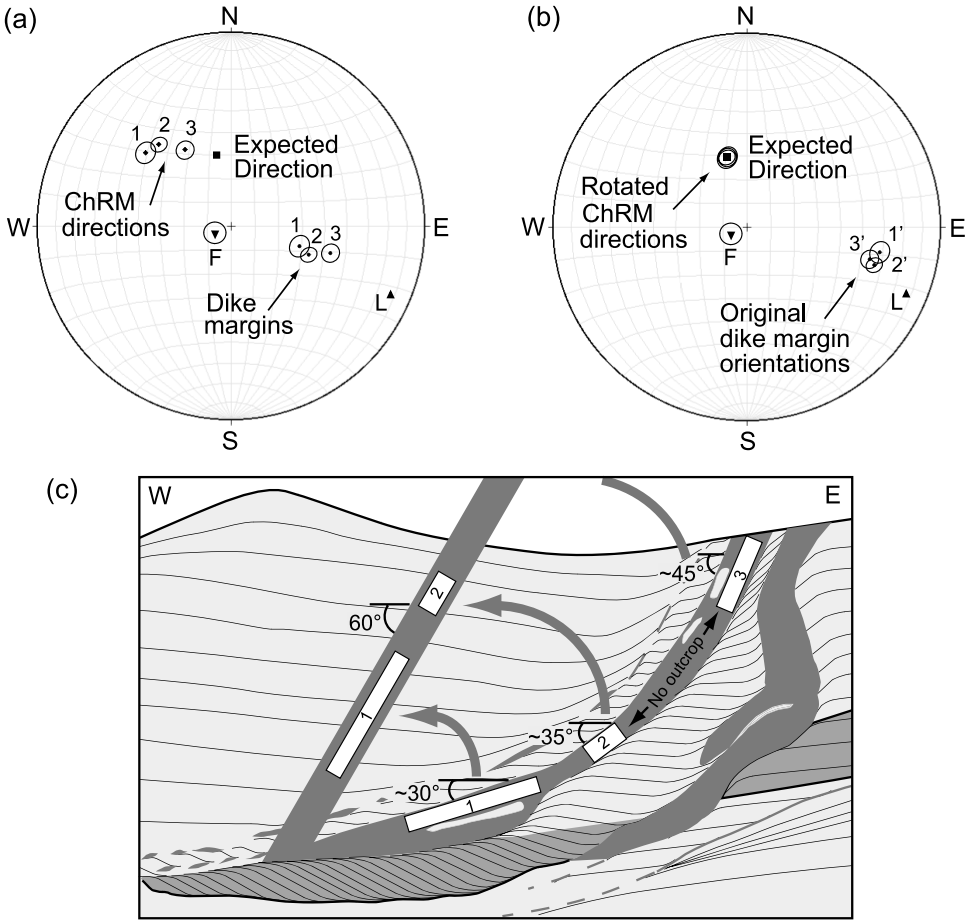

Figure 13. Structural reconstruction of dike 2 to its initial orientation. (a) Equal-area projection showing measured ChRM directions and poles to dike 2 margin orientations with α_{95} confidence limits. Expected direction for the Middle Eocene (declination, 346.1°; inclination, 58.69°) is from the study by *Besse and Courtillot* [1991]. L, mean stretching lineation in Marble Wash; F, pole to mean foliation. (b) Rotation of both the ChRM directions and the dike margin orientations about a horizontal north–south axis brings the ChRM directions into line with the Middle Eocene expected direction, while the dike margins coincide to give a single orientation of 011°W/60°W. (c) Schematic illustration showing dike 2 in both its present-day and reconstructed orientation.

calcite-dolomite thermometry to (1) place constraints on the style of deformation during each phase of deformation and (2) provide an independent indication of the temperatures under which this deformation occurred. EBSD analyses were carried out at the University of California-Santa Barbara (UCSB) using a JEOL 6300 scanning electron microscope fitted with an HKL Nordlys EBSD camera. Diffraction patterns were collected and indexed using CHANNEL 5 HKL software.

[34] First, we examined an east-directed shear band (Figures 14a–14d) to assess whether the smaller grains along the shear band show a crystallographic preferred orientation (CPO) consistent with dislocation glide or random crystallographic orientations that would be more consistent with grain boundary sliding, cataclasis, or both. For EBSD, the intensity of a fabric is defined by the multiple of uniform density (m.u.d.) and is quantified using the maximum intensity of the contoured pole figures. A maximum m.u.d. of 1 would represent a random fabric, whereas a maximum m.u.d. significantly greater than 1 would indicate the presence of a fabric. Figures 14c and 14d show that the smaller grains in the shear band do have a CPO (m.u.d. = 4.57),

Table 2. Carbonate Thermometry[a]

	X_{Mg}	X_{Ca}	X_{Mn}	X_{Fe}	T (°C)
Sample: FMW72 (East-Directed)					
Calcite A	0.033	0.959	0.002	0.006	456
Calcite B	0.026	0.967	0.002	0.005	412
Calcite C	0.029	0.964	0.002	0.005	431
Sample: FMW74 (West-Directed)					
Calcite A	0.020	0.979	0.000	0.001	347
Calcite B	0.019	0.980	0.000	0.001	344
Calcite C	0.021	0.978	0.000	0.001	362

[a]Each calcite composition listed is the average of five analyses. Temperatures were calculated using the method of *Anovitz and Essene* [1987].

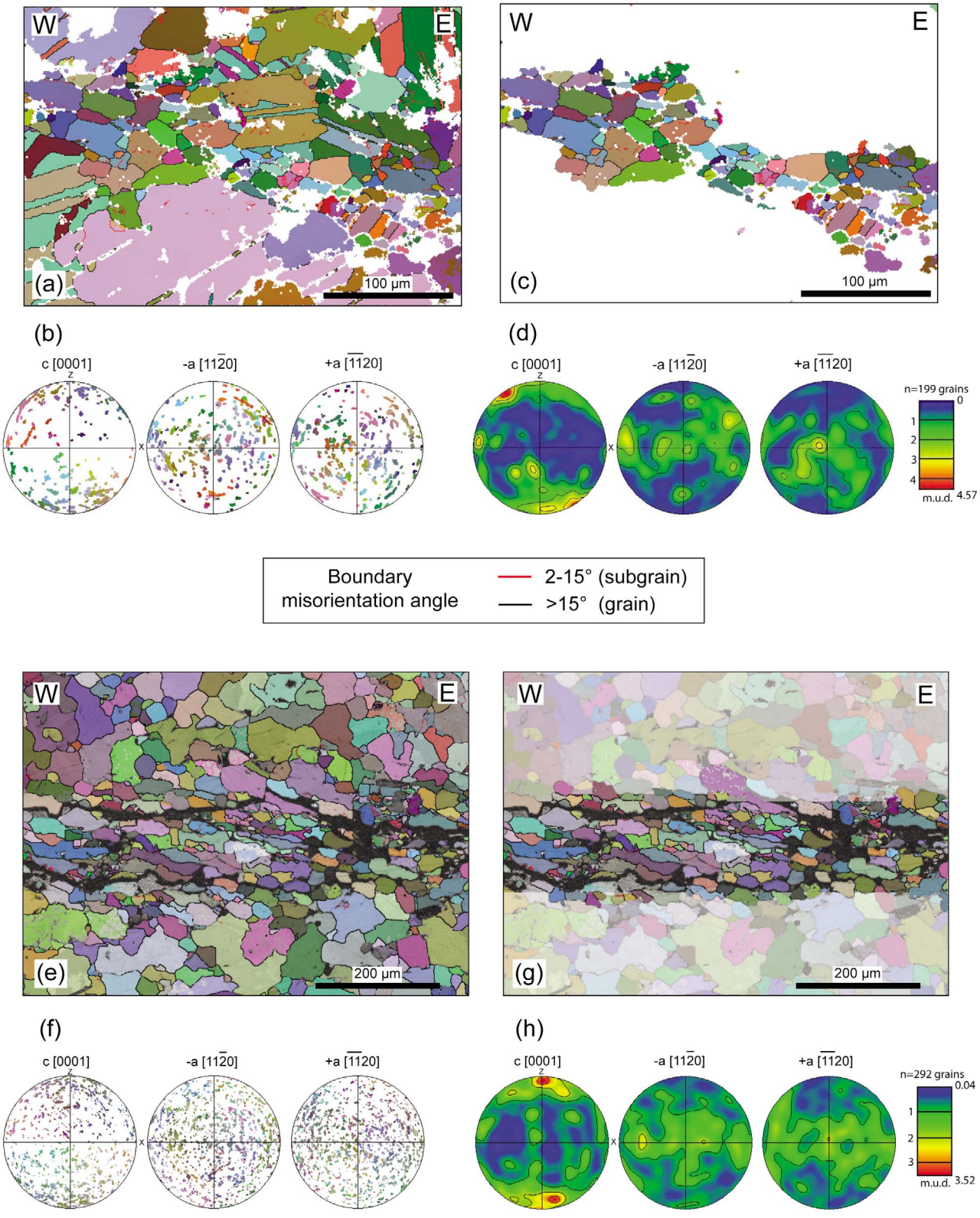
W
E
(a)
100 μm
(c)
100 μm
(b)
(d)
c [0001]
-a [11$\bar{2}$0]
+a [$\bar{1}$$\bar{1}$20]
n=199 grains
0
1
2
3
4
m.u.d. 4.57
Boundary misorientation angle
2-15° (subgrain)
>15° (grain)
(e)
200 μm
(g)
200 μm
(f)
(h)
n=292 grains
0.04
1
2
3
m.u.d. 3.52

Figure 14

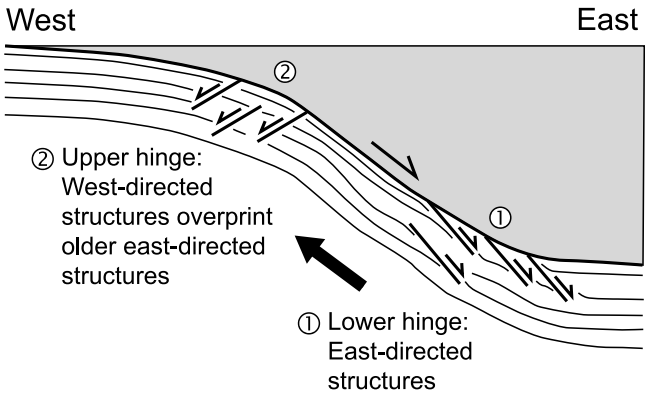

Figure 15. Schematic illustration to show how east- and west-directed structures could have formed as the footwall passed through two hinges with opposing senses of displacement during Tertiary exhumation. East-directed structures form early during passage through the lower hinge and are subsequently overprinted by west-directed structures as the footwall passes through the upper hinge. Modified from the study by *Axen et al.* [1995].

suggesting that deformation occurred at temperatures high enough for dislocation glide [*de Bresser and Spiers*, 1993], consistent with the calcite-dolomite thermometry results.

[35] Second, we carried out an identical study on a west-directed shear band (Figures 14e–14h; compare with Figure 8d). Again, the smaller grains within the shear band produced a CPO (m.u.d. = 3.52), consistent with temperatures high enough for dislocation glide and in agreement with the calcite-dolomite thermometry results.

[36] Further interpretation of the CPOs in these rocks is hindered by the effects of overprinting deformations and the difficulty in defining reference frames in rocks that have narrow shear bands oblique to the main foliation. Therefore, we conclude that the results of the calcite-dolomite thermometry and EBSD analyses indicate that both east- and west-directed phases of deformation in the mylonite zone occurred at temperatures below 500°C but high enough for ductile deformation in calcite.

4.2. Timing

[37] Two distinct episodes of footwall cooling identified in the northern Snake Range are interpreted to reflect two phases of tectonic exhumation: (1) late Eocene–early Oligocene and (2) early Miocene. The older phase of exhumation is constrained by stratigraphic data [*Gans and Miller*, 1983], dating of volcanic deposits [*Gans et al.*, 1989], and $^{40}Ar/^{39}Ar$ thermochronology [*Lee and Sutter*, 1991; *Lee*, 1995]. The final phase of exhumation is constrained by apatite and zircon fission track data, which indicate rapid cooling of footwall rocks to <50°C at 17 Ma [*Miller et al.*, 1999].

[38] *Lee* [1995] also noted that the thermochronological data indicate differential east–west cooling of the footwall within a given structural horizon: The northwestern flank of the range dropped below 300°C by 46 Ma and reached 115°C by 20 Ma, whereas the eastern parts of the range, where Marble Wash is located, were above 300°C until 19 Ma. Assuming that isotherms were subhorizontal during exhumation, this led *Lee* [1995] to postulate that the footwall rocks were exhumed by a rolling hinge fault system [*Buck*, 1988; *Wernicke and Axen*, 1988] in which the initially subhorizontal footwall units were tilted to the east during motion up a moderately dipping fault ramp [*Bartley and Wernicke*, 1984; *Lewis et al.*, 1999], cooled in this orientation, and then rolled back into a subhorizontal orientation at the surface as an isostatic response to hanging wall denudation. This would leave the resulting isochronal surfaces with a westerly dip.

5. Discussion

[39] The data presented in this paper lead us to make the following statements about the evolution of the northern Snake Range mylonite zone in Marble Wash. (1) Structural and paleomagnetic evidence indicates that the mylonite zone was formed by large-scale east-directed displacement after emplacement of the dikes at c. 40 Ma. (2) Structural relationships show that the east-directed mylonite zone was then overprinted by west-directed shear. (3) Geothermometry shows that west-directed shear followed east-directed shear during cooling through the interval 430°C–350°C. (4) Our own geochronological data and comparison with published $^{40}Ar/^{39}Ar$ data indicate that this history took place in the interval 40–19 Ma, prior to the final phase of exhumation and cooling indicated by fission-track data.

[40] The structural observations provide a clear picture of early east-directed deformation overprinted by later west-directed deformation. This is difficult to reconcile with the idea that the mylonites formed solely as a result of exhumation along the NSRD.

[41] On the basis of these conclusions, we consider three possible models for the formation of the northern Snake Range mylonite zone as a whole. However, our observations are limited to a small portion of the mylonite zone, and more

Figure 14. Calcite EBSD data. (a) Microstructure map of an east-directed shear band colored by the crystallographic orientations shown in Figure 14b. The horizontal axis lies parallel to the main mylonitic foliation (S_A) and to the ESE-trending stretching lineation of the bulk rock. Pixel spacing = 0.8 μm; 121,536 pixels in total. White areas were not indexed. (c) Microstructure map of smaller grains within the shear band. (d) Contoured lower hemisphere pole figures of the smaller grains show a crystallographic preferred orientation (CPO) consistent with deformation by dislocation glide in a ductile regime. (e) Microstructure map of a west-directed shear band (compare with Figure 8d), colored by orientations shown in Figure 14f. Again, the horizontal axis lies parallel to the main mylonitic foliation (S_A) and to the ESE-trending stretching lineation of the bulk rock. Pixel spacing = 1 μm; 291,036 pixels in total. (g) Microstructure map highlighting the smaller grains within the shear band. (h) Contoured lower hemisphere pole figures again show a CPO consistent with deformation by dislocation glide.

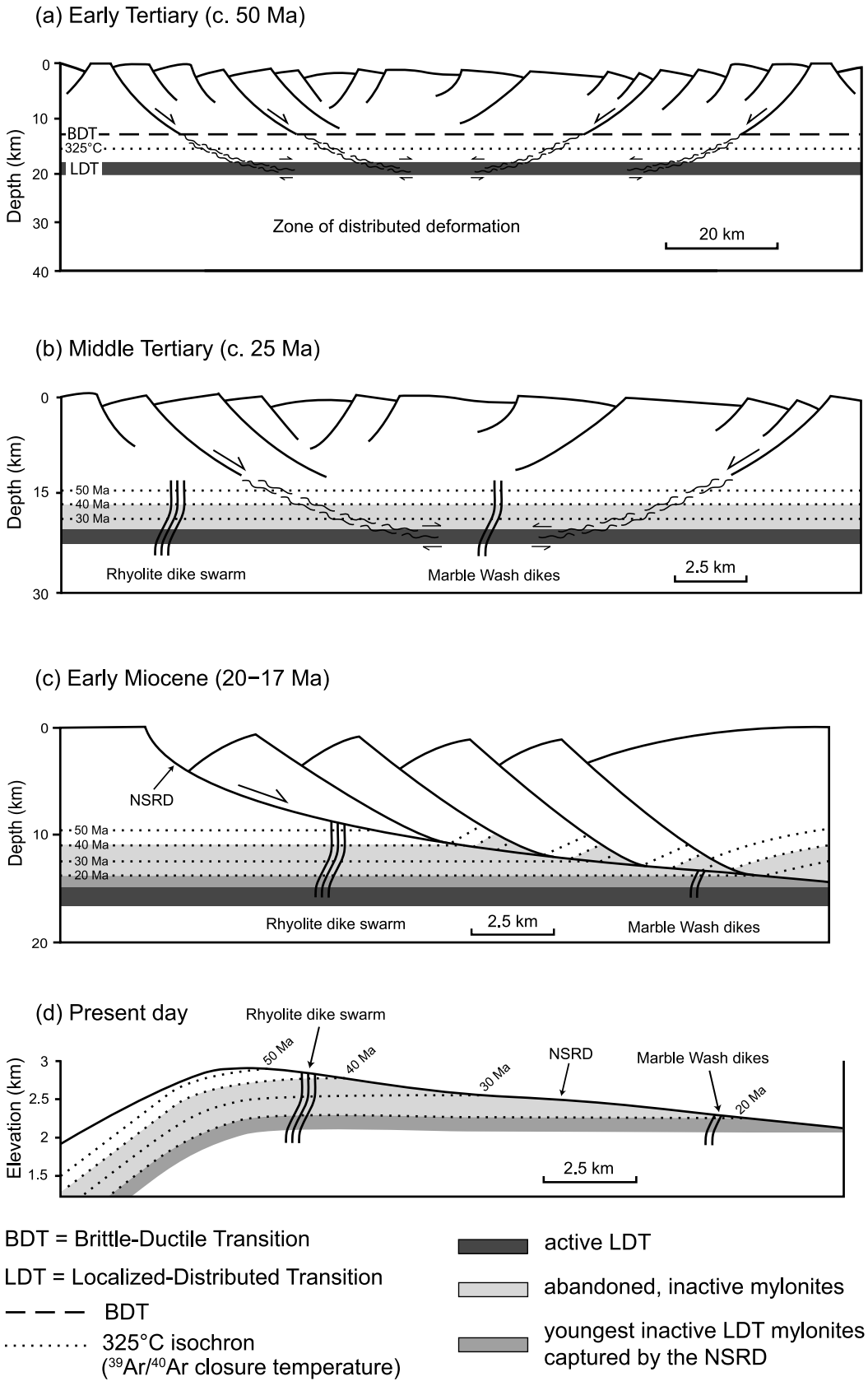
(a) Early Tertiary (c. 50 Ma)
Depth (km)
0
10
20
30
40
BDT
325°C
LDT
Zone of distributed deformation
20 km
(b) Middle Tertiary (c. 25 Ma)
Depth (km)
0
15
30
50 Ma
40 Ma
30 Ma
Rhyolite dike swarm
Marble Wash dikes
2.5 km
(c) Early Miocene (20−17 Ma)
Depth (km)
0
10
20
NSRD
50 Ma
40 Ma
30 Ma
20 Ma
Rhyolite dike swarm
2.5 km
Marble Wash dikes
(d) Present day
Rhyolite dike swarm
Elevation (km)
3
2.5
2
1.5
50 Ma
40 Ma
30 Ma
NSRD
Marble Wash dikes
20 Ma
2.5 km
BDT = Brittle-Ductile Transition
LDT = Localized-Distributed Transition
BDT
325°C isochron
(39Ar/40Ar closure temperature)
active LDT
abandoned, inactive mylonites
youngest inactive LDT mylonites
captured by the NSRD

Figure 16

studies are needed in other locations to confirm whether they can be applied to the entire range.

[42] 1. The opposing senses of shear recorded in the mylonite zone are related to movement of the footwall through the upper and lower hinges of a rolling hinge system, similar to structures seen in the Brenner Line normal fault zone in the eastern Alps [*Axen et al.*, 1995; *Selverstone et al.*, 1995]. As the footwall was exhumed, it passed first through a lower hinge, which created a top-east sense of shear, and second through an upper hinge, with an opposite, top-west sense of shear (Figure 15). The problem with this model is that, based on previous studies of, for example, the Brenner Line and the northern Snake Range detachment itself, the west-directed structures are likely to have formed near the surface (2–10 km depth in the Brenner line [*Selverstone et al.*, 1995] and about 3 km depth in the northern Snake Range [*Lee*, 1995]) and hence most probably in the brittle field. These shallow depths are inconsistent with the calculated temperatures and observed ductile style of west-directed deformation.

[43] 2. The mylonite zone represents counterflow of the deep crust toward an extensional breakaway zone, driven by a pressure gradient between the breakaway and the surrounding terrain [e.g., *Block and Royden*, 1990; *McKenzie et al.*, 2000; *McKenzie and Jackson*, 2002; *Wernicke*, 1992]. However, this would produce only an east-directed shear sense and, therefore, does not account for the observed west-directed shear. *MacCready et al.* [1997] described a late Eocene–Oligocene flow pattern in the migmatitic infrastructure immediately beneath the mylonite zone of the Ruby Mountains metamorphic core complex in north-central Nevada. This flow formed a fanning pattern inconsistent with the lineation direction of the mylonitic fabric, implying that flow and mylonitization were unrelated. No such contrast has been observed in the Snake Range.

[44] 3. The mylonite zone represents a midcrustal discontinuity between localized deformation above and distributed deformation below, which accumulated displacement from faults of various magnitudes and directions over time. This discontinuity was later captured by a moderately dipping normal fault that soled down into it and rolled it back into a subhorizontal orientation at the surface as a result of isostatic rebound [*Lee*, 1995]. In this interpretation the brittle hanging wall to the NSRD represents a series of rotated upper crustal normal fault blocks, and the ductile footwall represents an exhumed middle crustal discontinuity. This model fits best with our observations in the mylonite zone because it explains the presence of both east- and west-directed phases of motion, the greenschist-grade temperatures and associated ductile deformation, and the absence of the mylonite zone in the northwestern corner of the range.

[45] The schematic model shown in Figure 16 describes a possible evolution of the northern Snake Range mylonite zone based on the data presented in this paper and the thermochronological constraints of *Lee and Sutter* [1991], *Lee* [1995], and *Miller et al.* [1999]. We propose that initial crustal extension in the early Tertiary produced a subhorizontal midcrustal discontinuity within carbonate units (compare the rheologically controlled Raft River shear zone [*Wells*, 2001]), below the brittle-ductile transition, which separated upper and lower crustal domains extending in different ways. Above the transition, rocks deformed by motion along localized zones such as brittle faults or discrete ductile shear zones, transferring significant displacements downward into the discontinuity, whereas below the transition, deformation occurred by distributed coaxial crustal flow as proposed by *Lee et al.* [1987]. The transition itself was marked by a zone of high-strain rocks and mylonites. We refer to this discontinuity as the localized-distributed transition (LDT) (Figure 14a). In this interpretation, neither the sense nor amount of slip on the LDT need have been constant over its surface. The depth to the LDT would have depended primarily not only on temperature but also on rock and fluid composition. We assume here, for the purposes of discussion, that it formed a zone between the 400°C and 450°C isotherms (about 16–18 km in depth, assuming a geothermal gradient of 25°C/km).

[46] With continued extension and crustal thinning, the mylonites that formed below the LDT were progressively exhumed, migrating upward through the LDT (Figure 16b). As they cooled, ductile deformation ceased, creating a gradually thickening zone of abandoned mylonite above the LDT. Schematic $^{39}Ar/^{40}Ar$ cooling isochrons (interpreted to form at 325°C) are shown within this sequence in Figure 16b. At about 40 Ma, rhyolitic and mafic dikes were intruded into this sequence and deformed across the active LDT. Subsequent exhumation progressively deformed them further as structurally deeper levels rose up through the

Figure 16. (a) Initial crustal extension in the early Tertiary produces a subhorizontal midcrustal discontinuity, below the brittle–ductile transition, separating localized deformation above from distributed deformation below (localized-distributed transition (LDT)). Above the LDT, deformation is localized onto both east- and west-directed normal faults, which would probably alternate in time and space. (b) Continued extension into the middle Tertiary progressively exhumes the mylonites formed beneath the active LDT, creating a sequence of abandoned mylonite above it. At about 40 Ma, a suite of rhyolite and mafic dikes are intruded into this sequence and progressively deformed across the LDT while they too are exhumed. At about 25–20 Ma, an east-dipping normal fault soles into the LDT, followed by a later west-dipping normal fault. (c) The NSRD initiates in the early Miocene as a moderately dipping brittle normal fault that soles down to the middle crust, cutting from west to east through the sequence of successively abandoned LDT mylonites and both suites of dikes. (d) As the footwall is exhumed, the NSRD flexes around a rolling hinge as an isostatic response to hanging wall denudation, resulting in a subhorizontal footwall that cuts at a shallow angle across successive thermal isochrons (compare with Figure 2). Today, the approximately 1 km difference in structural elevation between the rhyolite dike swarm and the dikes in Marble Wash exposes the deformed levels of the Marble Wash dikes but conceals the same deformed levels of the rhyolite dikes at depth near the crest of the range.

active LDT (Figure 16b) (dike deformation below the 40 Ma isochron). At about 25–20 Ma, the mylonites exposed today in Marble Wash were formed when first an east-directed and later a west-directed normal-sense shear zone soled into the active LDT. This created first a dominant east-directed sense of displacement in the mylonites, as seen today and described by *Lee et al.* [1987], followed by a later, lower-temperature west-directed overprint. The lower temperature associated with this late-stage west-directed deformation meant that strain was more localized, and therefore, the west-directed overprint was confined to narrow shear bands that exploited preexisting weaknesses such as the dike margins. Continued thinning and cooling eventually stranded this superimposed east- and west-directed mylonitic deformation above the active LDT, where it was essentially "frozen in."

[47] Final exhumation began in the early Miocene (about 20–17 Ma) with the initiation of the NSRD as a moderately dipping brittle normal fault, as proposed by *Bartley and Wernicke* [1984], that soled down to the middle crust (Figure 16c). This fault cut from west to east through successively abandoned LDT mylonites, with the youngest (25–20 Ma) mylonites exposed in Marble Wash today. As the footwall was exhumed, the NSRD flexed around a rolling hinge as an isostatic response to hanging wall denudation, resulting in a subhorizontal footwall that cuts at a shallow angle across successive thermal isochrons (Figure 16d; compare with Figure 3). Today, the approximately 1 km difference in structural elevation between the rhyolite dike swarm and the Marble Wash dikes exposes the deformed levels of the dikes in Marble Wash but conceals the same deformed levels of the rhyolite dikes at depth near the crest of the range.

[48] In this interpretation, the brittle hanging wall to the NSRD represents a series of rotated upper crustal normal faults, whereas the ductile footwall represents a sequence of exhumed subhorizontal middle crustal discontinuities (LDTs) that have been tilted first to the east and then back into their present orientation during exhumation along the NSRD.

6. Conclusions

[49] Observations from a section of the northern Snake Range mylonite zone suggest that it may have originated as a subhorizontal discontinuity in the middle crust that separated upper and lower crustal domains responding to extension in different ways. Upper crustal rocks localized deformation along brittle faults or discrete shear zones, transferring significant displacements into the mylonite zone, whereas middle to lower crustal domains deformed by distributed crustal flow. Here we term this boundary the localized-distributed transition (LDT). In this interpretation, the sense of slip on the LDT need not have been constant over its surface, and the integrated displacement over the whole surface could have been small, or even zero. During extension, the mylonite zone rose toward the Earth's surface as the hanging wall thinned. Final exhumation occurred when slip on one of the hanging wall normal faults exceeded the remaining thickness of the upper crustal layer. As the mylonite zone was exhumed, the fault flexed around a rolling hinge, resulting in a subhorizontal geometry. In this interpretation, the brittle hanging wall represents a series of rotated upper crustal normal faults, whereas the ductile footwall represents one or more exhumed middle crustal discontinuities (LDTs).

[50] Comparable observations in the Whipple Mountains, the Betic Cordillera, and the Nordfjord–Sogn Detachment suggest that a similar exhumation history may be invoked in these areas. A recent thermomechanical model of core complex formation by *Tirel et al.* [2008] also supports a two-stage exhumation for some core complex mylonites. There is, however, no doubt that a detachment can exhume mylonites formed along a downdip ductile extension of the same fault (e.g., The Sierra Mazatán core complex, Sonora, Mexico [*Wong and Gans*, 2008]).

[51] **Acknowledgments.** We would like to thank Scott Bogue at Occidental College for the use of his paleomagnetic laboratory, Kevin McKeegan for his help with the UCLA ion microprobe, Frank Kyte for his assistance with the UCLA electron microprobe, and Brad Hacker at UCSB for the use of his EBSD facility. Snake Range field work would not have been possible without the help and support of the staff at the Great Basin National Park, in particular Ben Roberts and Matt Reece, and field assistance from Brad Foley and Geoffrey Pignotta. We thank Greg Davis, Jeff Lee, Elizabeth Miller, Robert Miller, Brian Wernicke, and two anonymous reviewers for their helpful and constructive reviews of this manuscript.

References

Anovitz, L. M., and E. J. Essene (1987), Phase equilibria in the system $CaCO_3$-$MgCO_3$-$FeCO_3$, *J. Petrol.*, *28*, 389–414.

Armstrong, R. L. (1972), Low-angle (denudation) faults, hinterland of the Sevier orogenic belt, Eastern Nevada, and Western Utah, *Geol. Soc. Am. Bull.*, *83*, 1729–1754.

Armstrong, R. L. (1982), Cordilleran metamorphic core complexes; from Arizona to southern Canada, *Annu. Rev. Earth Planet. Sci.*, *10*, 129–154.

Axen, G. J., and J. M. Bartley (1997), Field tests of rolling hinges; existence, mechanical types, and implications for extensional tectonics, *J. Geophys. Res.*, *102*, 20,515–20,537.

Axen, G. J., J. M. Bartley, and J. Selverstone (1995), Structural expression of a rolling hinge in the footwall of the Brenner Line normal fault, Eastern Alps, *Tectonics*, *14*, 1380–1392.

Bartley, J. M., and B. P. Wernicke (1984), The Snake Range decollement interpreted as a major extensional shear zone, *Tectonics*, *3*, 647–657.

Besse, J., and V. Courtillot (1991), Revised and synthetic apparent polar wander paths of the African, Eurasian, North American and Indian Plates, and true polar wander since 200 Ma, *J. Geophys. Res.*, *96*, 4029–4050.

Black, L. P., S. L. Kamo, I. S. Williams, R. Mundil, D. W. Davis, R. J. Korsch, and C. Foudoulis (2003), The application of SHRIMP to Phanerozoic geochronology; a critical appraisal of four zircon standards, *Chem. Geol.*, *200*(1–2), 171–188.

Block, L., and L. H. Royden (1990), Core complex geometries and regional scale flow in the lower crust, *Tectonics*, *9*, 557–567.

Buck, W. R. (1988), Flexural rotation of normal faults, *Tectonics*, *7*, 959–973.

Coney, P. J. (1974), Structural analysis of the Snake Range "decollement," East-Central Nevada, *Geol. Soc. Am. Bull.*, *85*, 973–978.

Coney, P. J. (1980), Cordilleran metamorphic core complexes; an overview, *Geol. Soc. Am. Mem.*, *153*, 7–31.

Cottle, J. M., M. J. Jessup, D. L. Newell, M. P. Searle, R. D. Law, and M. S. A. Horstwood (2007), Structural insights into the early stages of exhumation along an orogen-scale detachment: The South Tibetan Detachment System, Dzakaa Chu section, Eastern Himalaya, *J. Struc. Geol.*, *29*, 1781–1797.

Davis, G. A. (1988), Rapid upward transport of mid-crustal mylonitic gneisses in the footwall of a Miocene detachment fault, Whipple Mountains, southeastern California, *Geol. Rundsch.*, *77*, 191–209.

Davis, G. A., and G. S. Lister (1988), Detachment faulting in continental extension; perspectives from the Southwestern U.S. Cordillera, *Process. Cont. Lithosph. Deformation*, *218*, 133–159.

Davis, G. H. (1983), Shear-zone model for the origin of metamorphic core complexes, *Geology*, *11*, 342–347.

Davis, G. H., and P. J. Coney (1979), Geologic development of the Cordilleran metamorphic core complexes, *Geology*, *7*, 120–124.

de Bresser, J. H. P., and C. J. Spiers (1993), Slip systems in calcite single crystals deformed at 300–800°C, *J. Geophys. Res.*, *98*, 6397–6409.

Eaton, G. P. (1982), The Basin and Range Province; origin and tectonic significance, *Annu. Rev. Earth Planet. Sci.*, *10*, 409–440.

Gans, P. B., and E. L. Miller (1983), Style of mid-Tertiary extension in east-central Nevada, *in Geologic Excursions in the Overthrust Belt and Metamorphic Core Complexes of the Intermountain Region*, edited by K. D. Gurgel, pp. 107–160, *Utah Geol. Miner. Surv. Spec. Stud.*, Utah Geological and Mineral Survey, Salt Lake City, Utah.

Gans, P. B., G. A. Mahood, and E. R. Schermer (1989), Synextensional magmatism in the Basin and Range Province: A case study from the eastern Great Basin, *Geol. Soc. Am., Spec. Pap.*, *223*, 53.

Gans, P. B., E. L. Miller, C. C. Huggins, and J. Lee (1999a), Geologic map of the Little Horse Canyon Quadrangle, Nevada and Utah, Field Studies Map 20, Nev. Bur. Mines Geol., Reno, Nev.

Gans, P. B., E. L. Miller, and J. Lee (1999b), Geologic map of the Spring Mountain Quadrangle, Nevada and Utah, Field Studies Map 18, Nev. Bur. Mines Geol., Reno, Nev.

Gaudemer, Y., and P. Tapponnier (1987), Ductile and brittle deformations in the northern Snake Range, Nevada, *J. Struct. Geol.*, *9*, 159–180.

Hose, R. K., M. C. Blake Jr., and R. M. Smith (1976), Geology and mineral resources of White Pine County, Nevada, Nev. Bur. Mines Geol., Reno, Nev.

Lee, J. (1995), Rapid uplift and rotation of mylonitic rocks from beneath a detachment fault; insights from potassium feldspar $^{40}Ar/^{39}Ar$ thermochronology, northern Snake Range, Nevada, *Tectonics*, *14*(1), 54–77.

Lee, J., and J. F. Sutter (1991), Incremental $^{40}Ar/^{39}Ar$ thermochronology of mylonitic rocks from the northern Snake Range, Nevada, *Tectonics*, *10*, 77–100.

Lee, J., E. L. Miller, and J. F. Sutter (1987), Ductile strain and metamorphism in an extensional tectonic setting: A case study from the northern Snake Range, Nevada, USA, in *Continental Extensional Tectonics*, edited by M. P. Coward et al., pp. 267–298, Geol. Soc. Spec. Publ.

Lee, J., P. B. Gans, and E. L. Miller (1999a), Geologic map of the Mormon Jack Pass Quadrangle, Nevada, Field Studies Map 17, Nev. Bur. Mines Geol., Reno, Nev.

Lee, J., P. B. Gans, and E. L. Miller (1999b), Geologic map of the Third Butte East Quadrangle, Nevada, Field Studies Map 16, Nev. Bur. Mines Geol., Reno, Nev.

Lee, J., E. L. Miller, P. B. Gans, and C. C. Huggins (1999c), Geologic map of the Mount Moriah Quadrangle, Nevada, Field Studies Map 19, Nev. Bur. Mines Geol., Reno, Nev.

Lewis, C. J., B. P. Wernicke, J. Selverstone, and J. M. Bartley (1999), Deep burial of the footwall of the northern Snake Range decollement, Nevada, *Geol. Soc. Am. Bull.*, *111*, 39–51.

Lister, G. S., and G. A. Davis (1989), The origin of metamorphic core complexes and detachment faults formed during Tertiary continental extension in the northern Colorado River region, U.S.A., *J. Struct. Geol.*, *11*, 65–94.

Ludwig, K. R. (2001), User's Manual for Isoplot/Ex vers.2.2: A Geochronological Toolkit for Microsoft Excel, vol. 1a, *Berkeley Geochronolog. Cent. Spec. Pub.*, Berkeley Geochronological Center, Berkeley, Cal.

MacCready, T., A. W. Snoke, J. E. Wright, and K. A. Howard (1997), Mid-crustal flow during Tertiary extension in the Ruby Mountains core complex, Nevada, *Geol. Soc. Am. Bull.*, *109*, 1576–1594.

Mancktelow, N. S. (1985), The Simplon Line: A major displacement zone in the western Lepontine Alps, *Eclogae Geol. Helv.*, *78*, 73–96.

McKenzie, D., and J. Jackson (2002), Conditions for flow in the continental crust, *Tectonics*, *21*(6), 1055, doi:10.1029/2002TC001394.

McKenzie, D., F. Nimmo, J. A. Jackson, P. B. Gans, and E. L. Miller (2000), Characteristics and consequences of flow in the lower crust, *J. Geophys. Res.*, *105*, 11,029–11,046.

Miller, E. L., and P. B. Gans (1999), Geologic map of the Cove Quadrangle, Nevada, Field Studies Map 22, Nev. Bur. Mines Geol., Reno, Nev.

Miller, E. L., P. B. Gans, and J. Garing (1983), The Snake Range decollement: An exhumed mid-Tertiary ductile-brittle transition, *Tectonics*, *2*, 239–263.

Miller, E. L., P. B. Gans, J. E. Wright, and J. F. Sutter (1988), Metamorphic history of the east-central Basin and Range Province; tectonic setting and relationship to magmatism, in *Rubey Colloquium on Metamorphism and Crustal Evolution of the Western United States*, edited by W. G. Ernst, pp. 649–682, Prentice-Hall, Upper Saddle River, N.J.

Miller, E. L., T. A. Dumitru, R. W. Brown, and P. B. Gans (1999), Rapid Miocene slip on the Snake Range–Deep Creek Range fault system, east-central Nevada, *Geol. Soc. Am. Bull.*, *111*, 886–905.

Misch, P., and J. C. Hazzard (1962), Stratigraphy and metamorphism of Late Precambrian rocks in central northeastern Nevada and adjacent Utah, *Am. Assoc. Pet. Geol. Bull.*, *46*, 289–343.

Misch, P. H. (1960), Regional structural reconnaissance in central-northeast Nevada and some adjacent areas: Observations and interpretations, *Int. Assoc. Petrol. Geol. 11th Ann. Field Conf., Guidebook*, 17–42, International Association of Petroleum Geologists.

Paces, J. B., and J. D. Miller Jr. (1993), Precise U-Pb ages of Duluth Complex and related mafic intrusions, northeastern Minnesota; geochronological insights to physical, petrogenetic, paleomagnetic, and tectonomagnetic processes associated with the 1.1 Ga Midcontinent Rift System, *J. Geophys. Res.*, *98*, 13,997–14,013.

Platt, J. P., and J. H. Behrmann (1986), Structures and fabrics in a crustal-scale shear zone, Betic Cordillera, SE Spain, *J. Struct. Geol.*, *8*, 15–34.

Selverstone, J., G. J. Axen, and J. M. Bartley (1995), Fluid inclusion constraints on the kinematics of footwall uplift beneath the Brenner Line normal fault, Eastern Alps, *Tectonics*, *14*, 264–278.

Tirel, C., J.-P. Brun, and E. Burov (2008), Dynamics and structural development of metamorphic core complexes, *J. Geophys. Res.*, *113*, B04403, doi:10.1029/2005JB003694.

Wells, M. L. (2001), Rheological control on the initial geometry of the Raft River detachment fault and shear zone, western United States, *Tectonics*, *20*(4), 435–457.

Wernicke, B. (1981), Low-angle normal faults in the Basin and Range Province: Nappe tectonics in an extending orogen, *Nature*, *291*, 645–647.

Wernicke, B. (1992), Cenozoic extensional tectonics of the U.S. Cordillera, in *The Cordilleran Orogen: Conterminous U.S.*, edited by B. C. Burchfiel, P. W. Lipman, and M. L. Zoback, Geological Society of America, G-3, Boulder, Col.

Wernicke, B. P., and G. J. Axen (1988), On the role of isostasy in the evolution of normal fault systems, *Geology*, *16*, 848–851.

Winter, J. D. (2001), *An Introduction to Igneous and Metamorphic Petrology*, 697 pp., Prentice-Hall, Upper Saddle River, N.J.

Wong, M. S., and P. B. Gans (2008), Geologic, structural, and thermochronologic constraints on the tectonic evolution of the Sierra Mazatán core complex, Sonora, Mexico: New insights into metamorphic core complex formation, *Tectonics*, *27*, TC4013, doi:10.1029/2007TC002173.

F. J. Cooper, School of Earth and Space Exploration, Arizona State University, Tempe, AZ 85287, USA. (frances.cooper@asu.edu)

M. J. Grove, School of Earth Sciences, Stanford University, Stanford, CA 94305, USA.

J. P. Platt and E. S. Platzman, Department of Earth Sciences, University of Southern California, Los Angeles, CA 90089, USA.

G. Seward, Department of Earth Science, University of California, Santa Barbara, CA 93106, USA.